processes

MDPI

Article

Numerical Analysis of Effects of Specularity Coefficient and Restitution Coefficient on the Hydrodynamics of Particles in a Rotating Drum

Rezwana Rahman [1], Haiping Zhu [1,*] and Aibing Yu [2]

[1] School of Engineering, Design and Built Environment, Western Sydney University, Locked Bag 1797, Penrith, NSW 2751, Australia; R.Rahman3@westernsydney.edu.au
[2] Faculty of Engineering, Monash University, 14 Alliance Lane (Engineering 72), Clayton, VIC 3168, Australia; Aibing.Yu@monash.edu.au
* Correspondence: h.zhu@westernsydney.edu.au; Tel.: +61-2-9685-4609

Abstract: Various simulations have been conducted to understand the macroscopic behavior of particles in the solid-gas flow in rotating drums in the past. In these studies, the no-slip wall boundary condition and fixed restitution coefficient between particles were usually adopted. The paper presents a numerical study of the gas-solid flow in a rotating drum to understand the effect of the specularity coefficient and restitution coefficient on the hydrodynamic behavior of particles in the segregation process. The volume fraction, granular pressure, granular temperature and their relationships are examined in detail. The boundary conditions of the no-slip and specularity coefficient of 1 are compared. In the simulations, two different sizes of particles with the same density are considered and the Eulerian–Eulerian multiphase model and the kinetic theory of granular flow (KTGF) are used. The results reveal that the hydrodynamical behavior of the particles in the rotating drum is affected by the boundary condition and restitution coefficient. In particular, the increase of specularity coefficient can increase the active region depth, angle repose, granular pressure for both small and large particles and granular temperature for large particles. With increasing restitution coefficient, the angle of repose decreases and granular pressure and temperature increase at the same volume fraction for both small and large particles.

Keywords: rotating drum; gas–solids flow; computational fluid dynamics; granular pressure; granular temperature

Citation: Rahman, R.; Zhu, H.; Yu, A. Numerical Analysis of Effects of Specularity Coefficient and Restitution Coefficient on the Hydrodynamics of Particles in a Rotating Drum. *Processes* **2022**, *10*, 167. https://doi.org/10.3390/pr10010167

Academic Editor: Ireneusz Zbicinski

Received: 19 December 2021
Accepted: 13 January 2022
Published: 15 January 2022

1. Introduction

Understanding the dynamical behaviour of particles in rotating drums has attracted numerous research efforts over the past few decades due to their extensive applications in process industries [1–3]. Knowledge of the solids flow pattern in rotating drums is essential to the optimization of drum design. In general, different flow regimes of solid motion can be exhibited by adjusting the rotational speed of drums [4]. For a rolling motion, there are two distinct regions: passive and active, in which particle mixing and segregation occur. The formation of different segregation patterns and the mechanism are still not fully understood though many studies have been conducted in this area [5–7].

The dynamics of granular in the segregation process is complex and it is related to the properties of particles and the boundary condition of the systems [8,9]. Two of the key properties affecting the particle behaviour are the specularity coefficient and restitution coefficient. Specularity coefficient was defined by Johnson and Jackson [10] for the wall boundary condition, i.e., the relative velocity between particles and wall, which is also known as slip velocity. It ranges from 0 to 1, with the specularity coefficient of 1 often being considered to be the no-slip wall boundary condition [11]. The restitution coefficient is the ratio of the final to initial relative velocity between two particles after they collide.

The value of the restitution coefficient between particles depends on the impact velocity of particles, particles' physical properties and hardness ratio [12,13]. Many researchers have conducted simulations to investigate the hydrodynamics of particles in rotating drums, especially by using computational fluid dynamics (CFD) [2,14–16]. In these studies, the no-slip wall boundary condition was normally adopted. However, such a boundary condition rarely exists in real systems. A few studies have been carried out to understand the effect of the specularity coefficient on the dynamics of particles in rotating drums. Huang and Kuo [17] conducted simulations to study the impact of the specularity coefficient in the segregation process in a rotating drum. Machado et al. [18] simulated the particle dynamic flow in a rotary drum with one flight under different boundary conditions by using the Euler-Euler approach with the kinetic theory of granular flow. These studies were mainly focused on the volume fraction and velocity distribution of the particles. The effects of the specularity coefficient on the hydrodynamical behaviour in terms of other properties such as granular pressure and temperature are still unclear. In addition, very little investigation has been conducted to understand the difference in particle behaviour between the no-slip and specularity coefficient boundary conditions for a binary particle segregation in rotating drums. The effect of the restitution coefficient has not been paid much attention in the past although it is one of the key properties in the CFD simulation of gas–solid flow in rotating drums. Taghizadeh [19] conducted numerical simulation by using the CFD to explore the effect of restitution coefficient on granular temperature by considering single sized particles. However, this does not give a clear picture on how the restitution coefficient can impact the granular temperature in the segregation process where the sizes of the particles are different. Moreover, very little is known about the effect of the restitution coefficient on the hydrodynamics of particles such as volume fraction, granular temperature, granular pressure and the relationships among them.

In this work, CFD simulations have been conducted to study the effect of the specularity coefficient and the restitution coefficient between particles on the hydrodynamics of gas–solids flow in a rotating drum. The granular pressure and granular temperature of large and small particles in the segregation process are examined in detail. The boundary conditions with the no-slip and specularity coefficients 1 and 0.65 are considered. The results obtained based on the different boundary conditions are compared. Especially, the difference between the no-slip and specularity coefficient 1 in the flow is elucidated. The effects of the restitution coefficient on the granular pressure and granular temperature are investigated.

2. Simulation Method and Conditions

The gas-solid flow in a rotating drum was simulated using the KTGF (Kinetic theory of granular flows)–Eulerian approach in this work. In the method, the governing equations consist of the continuity equations of mass, balances equations of momentum for both gas and solids phases and the balance equations for the granular temperature for solid phases. A binary mixture consisting of particles with two different sizes was considered. The equations of continuity for the gas and solids phases are respectively given by

$$\frac{\partial}{\partial t}(\alpha_g \rho_g) + \nabla \cdot \left(\alpha_g \rho_g \vec{v}_g\right) = 0 \tag{1}$$

$$\frac{\partial}{\partial t}(\alpha_{si} \rho_{si}) + \nabla \cdot \left(\alpha_{si} \rho_{si} \vec{v}_{si}\right) = 0 \tag{2}$$

where ρ, α and v are the density, volume fraction and velocity of each phase, respectively. The subscripts si (i = 1, 2) and g denote the ith component of the solids phase and gas phase, respectively. The sum of the volume fractions of each phase equals to unity:

$$\alpha_g + \sum_{i=1}^{2} \alpha_{si} = 1 \tag{3}$$

The balance equations of momentum for the gas and the solids phases are respectively,

$$\begin{aligned} \frac{\partial}{\partial t}\left(\alpha_g \rho_g \vec{v}_g\right) + & \quad \nabla\cdot\left(\alpha_g \rho_g \vec{v}_g \vec{v}_g\right) \\ & = -\alpha_g \nabla p + \nabla\cdot\bar{\bar{\tau}}_g + \sum_{i=1}^{2} K_{sig}\left(\vec{v}_{si} - \vec{v}_g\right) + \alpha_g \rho_g \vec{g} \\ \frac{\partial}{\partial t}\left(\alpha_{si} \rho_{si} \vec{v}_{si}\right) + & \quad \nabla\cdot\left(\alpha_{si} \rho_{si} \vec{v}_{si} \vec{v}_{si}\right) \\ & = -\alpha_{si} \nabla p - \nabla p_{si} + \nabla\cdot\bar{\bar{\tau}}_{si} + K_{gsi}\left(\vec{v}_g - \vec{v}_{si}\right) \end{aligned} \tag{4}$$

$$+ K_{sjsi}\left(\vec{v}_{sj} - \vec{v}_{si}\right) + \alpha_{si} \rho_{si} \vec{g} \qquad for\ i \neq j \tag{5}$$

where p and p_{si} are the gas phase pressure and the solid phase pressure of the ith component, respectively; $\vec{g}$ represents the gravitational acceleration; K_{sig}, K_{gsi} and K_{sjsi} are the interphase interaction terms. $\bar{\bar{\tau}}$ is the stress-strain tensor.

The balance equations for the granular temperature are given by:

$$\begin{aligned} \frac{3}{2}\left[\frac{\partial}{\partial t}\left(\alpha_{si} \rho_{si} \theta_{si}\right) + \nabla\cdot\left(\alpha_{si} \rho_{si} \vec{v}_{si} \theta_{si}\right)\right] &= \left(-p_{si}\bar{\bar{I}} + \bar{\bar{\tau}}_{si}\right) : \nabla \vec{v}_{si} \\ + \nabla\cdot\left(k_{\theta_{si}} \nabla \theta_{si}\right) - \gamma_{\theta_{si}} + \varphi_{gsi} + \varphi_{sjsi},\ & \text{for } i \neq j \end{aligned} \tag{6}$$

where θ_{si} denotes the granular temperature; $\bar{\bar{I}}$ is the unit vector; $k_{\theta_{si}}$ is the diffusion coefficient; $\gamma_{\theta_{si}}$ is the rate of collisional energy dissipation; φ_{gsi} and φ_{sjsi} are the energy exchanges between gas and solid phases and between solid phases, respectively.

The solids pressure consists of a kinetic term and a collision term:

$$p_{si} = \alpha_{si} \rho_{si} \theta_{si} + 2\frac{d_{sjsi}^3}{d_{si}^3}\left(1 + e_{sjsi}\right)\ \alpha_{si} \alpha_{sj} \rho_{si} g_{0,sjsi} \theta_{si} \tag{7}$$

where e_{sjsi} is the restitution coefficient between particles; d_{si} is the particle diameter of the ith component; d_{sjsi} (= $\left(d_{sj} + d_{si}\right)/2$) is the mean value of the two particle diameters. $g_{0,sjsi}$ is the radial distribution function, given by

$$\begin{aligned} g_{0,sisj} &= \frac{d_{si} g_{0,sjsj} + d_{sj} g_{0,sisi}}{d_{si} + d_{sj}} \\ g_{0,sisi} &= \left[1 - \left(\frac{\alpha_s}{\alpha_{s,max}}\right)^{\frac{1}{3}}\right]^{-1} + \frac{1}{2} d_{si} \sum_{i=1}^{2} \frac{\alpha_{si}}{d_{si}} \end{aligned}$$

where $\alpha_s = \sum_{i=1}^{2} \alpha_{si}$ and $\alpha_{s,max}$ is the volume fraction α_s at a closely random packing state.

The no-slip boundary condition has been used for gas phase, i.e., the relative movement between the wall and gas is zero. Both the no-slip and slip boundary conditions have been considered for the solid phase. For no-slip condition, it is assumed that the slip velocities of particles at the wall are zero. For the wall slip condition, Johnson and Jackson boundary conditions [10] are applied:

$$\frac{\vec{u}_{sl}\cdot\left(\bar{\bar{\sigma}}_c + \bar{\bar{\sigma}}_f\right)\cdot\vec{n}}{\left|\vec{u}_{sl}\right|} + \frac{\varnothing\sqrt{3\theta_s}\pi\rho_s\alpha_s\left|\vec{u}_{sl}\right|}{6\alpha_{s,max}\left[1 - \left(\frac{\alpha_s}{\alpha_{s,\,max}}\right)^{\frac{1}{3}}\right]} + N_f \tan\delta = 0 \tag{8}$$

where $\vec{u}_{sl}$ is the slip velocity between the wall and particles; $\bar{\bar{\sigma}}_c$ and $\bar{\bar{\sigma}}_f$ are the collisional and frictional stress tensors, respectively; $\vec{n}$ is the unit normal vector of the wall; ϕ is the specularity coefficient; θ_s (= $\sum_{i=1}^{2} \theta_{si}$) is the granular temperature; ρ_s (= $\sum_{i=1}^{2} \rho_{si}$) is the density

of the solid phases; N_f is the frictional pressure; and δ is the angle of friction between the wall and particles.

A higher order scheme, i.e., QUICK scheme, has been used to solve the balance equations. The solutions of pressure and velocity obtained from the equations need corrections. The SIMPLE algorithm has been used for the corrections in every iteration.

In this work, a horizontal rotating drum with a diameter of 50 mm and a length of 50 mm has been considered (Figure 1a). The drum is similar to that used in [17], where the segregation pattern and velocity distribution were focused on. It rotates clockwise with a speed of 20 rpm. Under this condition, the flow of the drum is in the rolling mode. In this mode, there are two distinct flow regions: passive and active (Figure 1b). In the CFD (FLUENT) finite volume numerical analysis, the drum volume is divided into 29, 588 elements (Figure 1c). Simulations with more elements have been conducted. It has been shown that the results are not affected by the number of elements, confirming that the present treatment is suitable for the system considered. Other parameters used in the simulations are provided in Table 1.

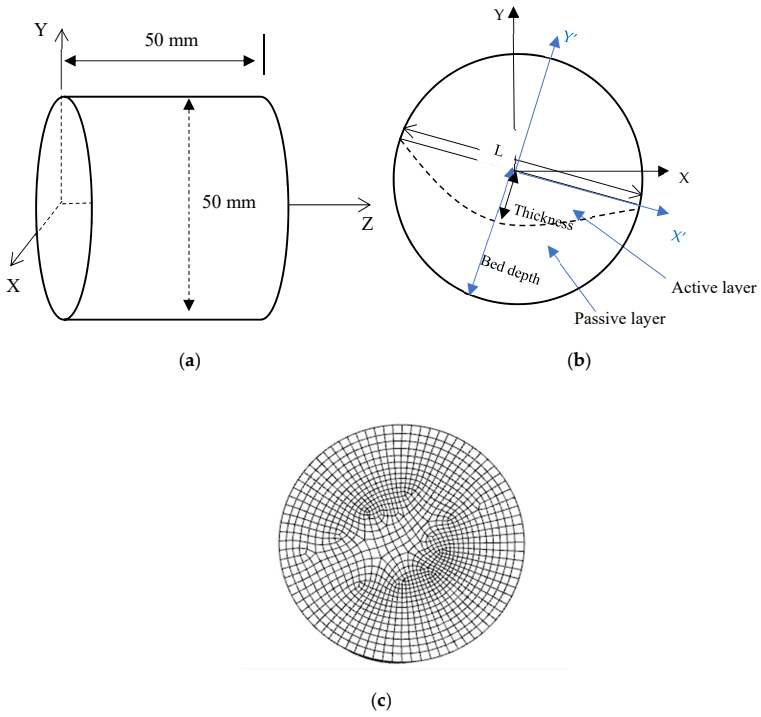

Figure 1. (**a**) Schematic diagram of the rotating drum; (**b**) rolling mode of particles' motion in a transverse plane of the rotating drum; and (**c**) mesh of the transverse plane.

Table 1. Parameters used in the simulations.

Quantity	Value
Solid density, ρ_s (kg/m^3)	2500
Particle diameter, d_s (mm)	0.385, 0.775
Angle of internal friction, ϕ°	23.94°, 33.66°
Particle-particle restitution coefficient, e_p	0.9
Particle-wall restitution coefficient, e_w	0.9
Air density, ρ_g (kg/m^3)	1.225
Cylinder diameter, D (mm)	50
Cylinder length, L (mm)	50
Rotational speed, ω (rpm)	20
Boundary condition	0.65, 1 (specularity coefficient), no-slip
Restitution coefficient	0.75, 0.8, 0.9

In each simulation, the smaller particles are initially horizontally loaded on the top of the larger particles. Two streams of particles in the drum are of equal volume and the total solids fill level is 50%. The initial volume fraction is 0.61 for both particle streams. The remaining spaces are filled with gas (air was used as the gas phase here). The interstitial air has a density 1.225 kg/m^3 and viscosity 1.7894 $\times$ 10^{-5} kg/(m·s). The simulation time step is 10^{-4} s and the total simulation time is 5 s. The simulations have also been run a longer time. The results show that the properties considered are very close at 5 s and 15 s, which implies that a steady state has been reached at 5 s for all cases.

3. Results and Discussion

3.1. Volume Fraction and Velocity

Figure 2 shows the distributions of the volume fraction at different times for the flow with the no-slip boundary condition and 0.9 restitution coefficient. The particulate phase distribution mainly depends on the momentum transferring between the drum walls and particles and that between particles in a horizontal rotating drum. At the no-slip boundary condition, high momentum is transferred by the wall to the particles, which causes fast motions of the particles. Therefore, the particles could form a segregation core after a short period of time as shown in Figure 2. Particle percolation can be observed: small particles gradually concentrating at the centre of the bed, while larger particles accumulating near the drum wall. At t = 5 s, a segregation pattern is formed, i.e., a segregation band formed by the large particles near the wall and a segregation core formed by the small particles at the centre region of the bed. The segregation profile is similar to the one obtained in the previous studies [17].

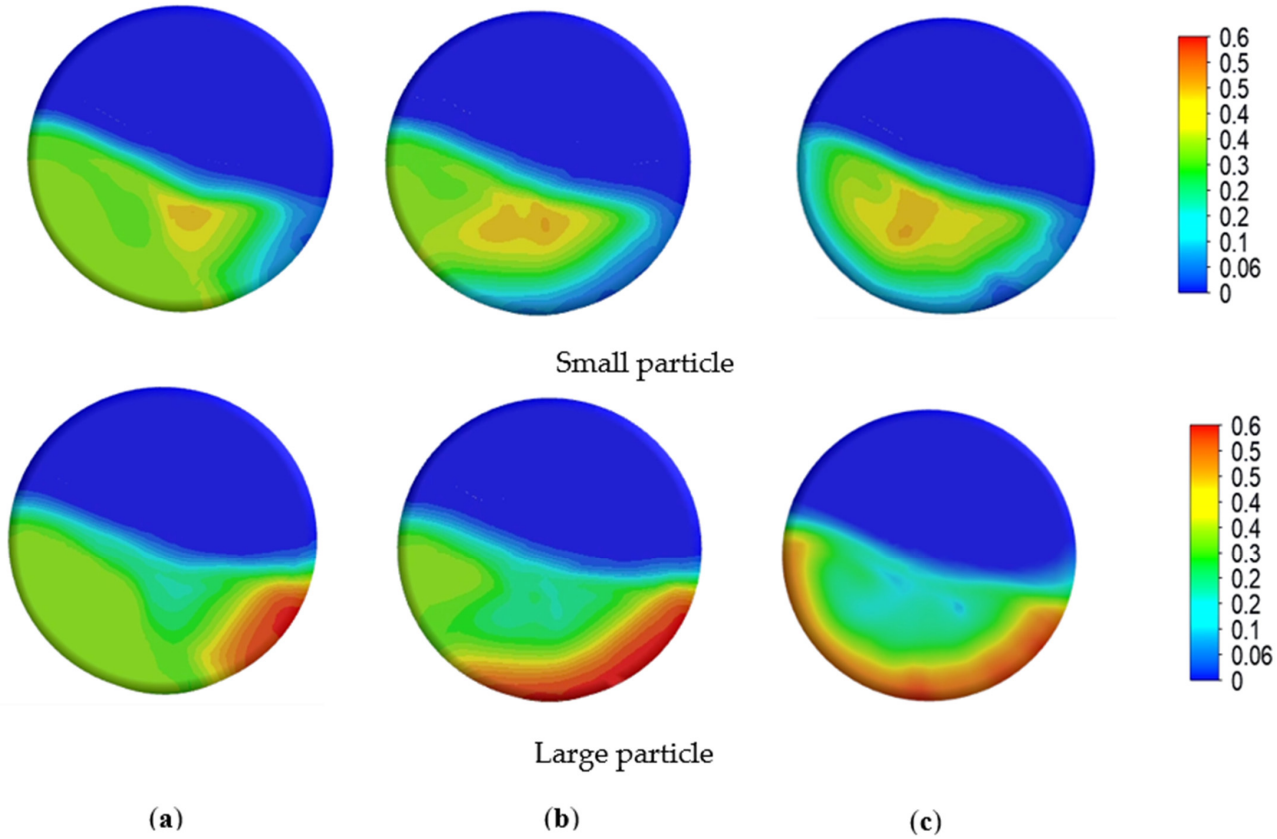

Figure 2. Distributions of the volume fraction of small and large particles for the no-slip boundary condition and 0.9 restitution coefficient at different instants of time: (**a**) 0.5 s; (**b**) 2 s and (**c**) 5 s.

Figure 3 shows the segregation pattern of particles for different boundary conditions, including those with the no-slip and specularity coefficients 1 and 0.65. The radial segrega-

tion profiles are similar in all cases for both the sizes of particles. The small particle rich core is formed at the bed centre while the large particles form a rich band near the wall wrapping up the small particle core. Compared with specularity coefficients 1 and 0.65, the no-slip boundary condition creates a thicker segregation band near the wall. The volume fraction is higher at the band region for the no-slip condition due to more momentum transferring between the wall and particles. Less time is required to form the segregation core for both the sizes of particles at this condition.

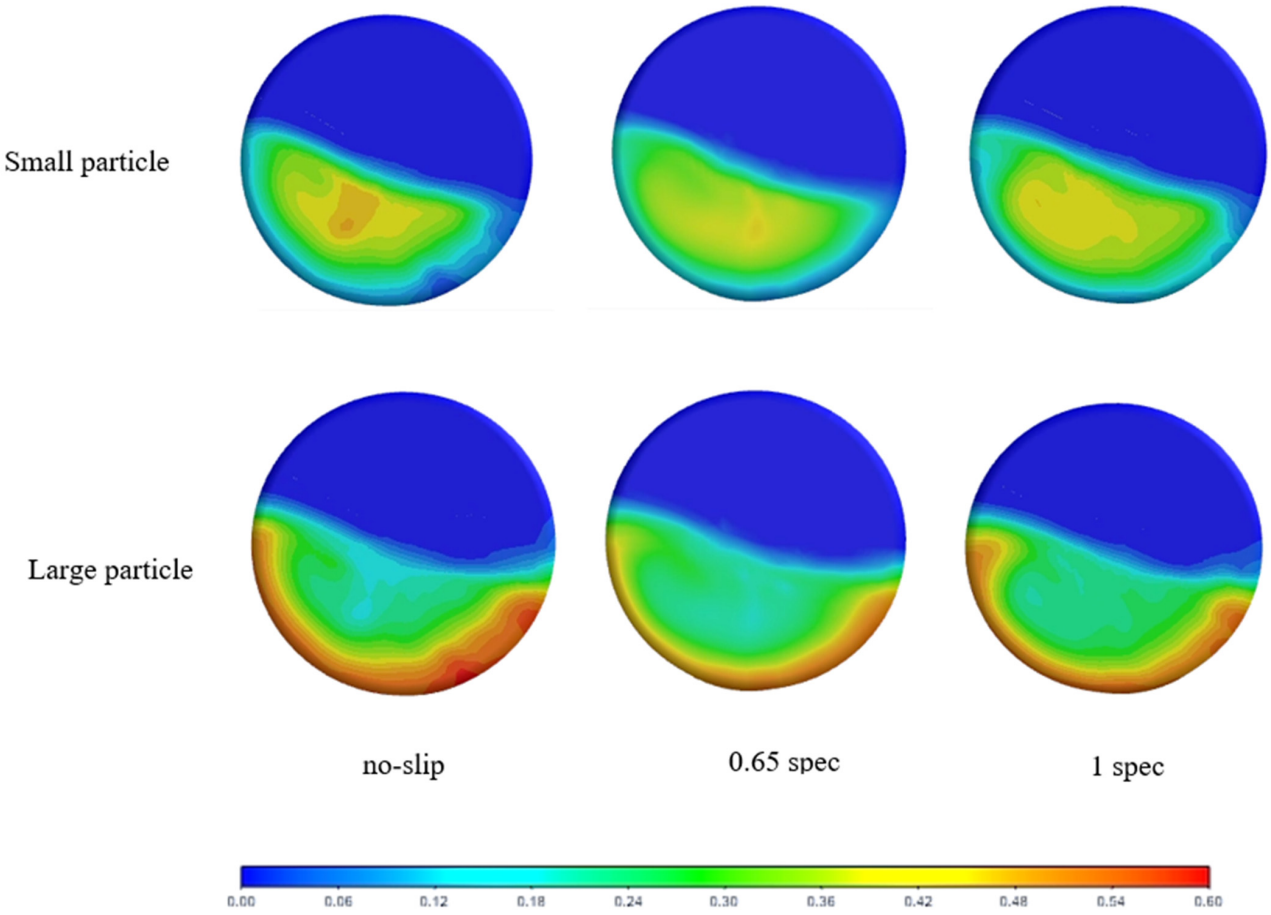

Figure 3. Solid volume fraction distributions in the rotating drum with different specularity coefficients for small and large particles at t = 5 s. "spec" represents "specularity coefficient".

Figure 4 shows the effect of restitution coefficient on the formation of the particle segregation pattern. The same wall boundary condition has been adopted in these cases. So, the main contribution to the formation of segregation core and band is from the momentum transferring between particles. Compared with the restitution coefficient of 0.9, for the two lower restitution coefficients, the momentum transferring is smaller, or the relative velocity of two particles after they collide become lower. This causes that more time needs to form a stable segregation core for small particles and segregation band for large particles. The effect of the restitution coefficient on the profile of the volume fraction is obvious, as shown in Figure 4. Different from restitution coefficient 0.9, for the two lower restitution coefficients, there is a small region near the middle of the bed, in which large particles concentrate.

The streamwise velocity and angle of repose are two important properties for understanding the hydrodynamic behaviour of particles in a rotating drum. Figure 5 shows the streamwise velocity Vx as a function of the bed depth (along the Y′ axis) for large particles at t = 5 s for different boundary conditions and restitution coefficients. For all cases considered, the velocity profile can be divided into two segments, one exhibiting a linear

trend, another being nonlinear. The two segments correspond to the passive and active regions, respectively, and intersect at the point with zero velocity except the cases with restitution coefficients of 0.75 and 0.8. At the intersection, the velocity profile has a large change in its gradient. In the active region, the velocity increases along the Y′ axis from the intersection and reach its highest magnitude at the surface of the bed for both small and large particles. In the passive region, the velocity decreases along the Y′ axis from the wall. Among the three boundary conditions, specularity coefficient 1 has the largest velocity, while specularity coefficient 0.65 has the lowest one. The depth of the active region is higher for specularity coefficient 1 and lower for specularity coefficient 0.65. This is because the particles near the wall are brought to a higher location by the wall for a larger specularity coefficient. These particles move down along the bed surface from such a height, resulting in bigger magnitude of particle velocity. The case with restitution coefficient 0.9 has larger velocities in the active region compared with restitution coefficients 0.7 and 0.8. Different from the other cases, in the two cases with lower restitution coefficients, the two segments of the velocity profile intersect at a point with a positive velocity Vx. The reason is that for the two cases, besides the segregation band near the wall, an additional concentration region is formed inside the bed by the large particles. Most of these particles have small positive velocities.

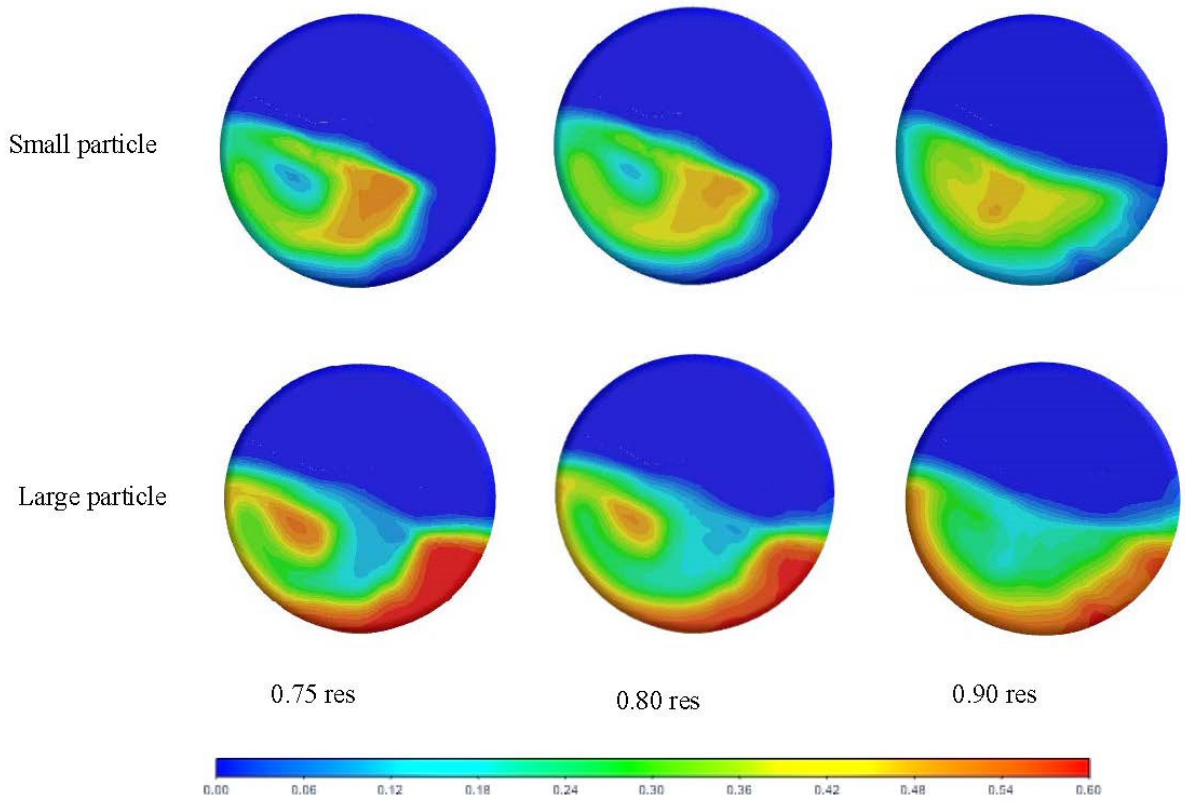

Figure 4. Solid volume fraction distributions in the rotating drum with different restitution coefficients for the small and large particles at t = 5 s. "res" represents "restitution coefficient".

The value of the angle of repose is affected by the boundary condition and restitution coefficient as shown in Figure 6. The no-slip boundary condition has a higher angle of repose than the cases with specularity coefficients 1 and 0.65. This is because the no-slip condition between the wall and particles can cause the particles to move to a high position along the wall. With the increasing restitution coefficient, the angle of repose decreases. The reason for the feature is that for the same boundary condition, there are higher particle velocities on the bed surface for larger restitution coefficient as shown in Figure 5b. When the particles with a larger velocity Vx move down along the free-flowing bed surface,

they collide with the drum wall and create more momentum to resist the motions of other particles, leading to a lower gradient of bed surface.

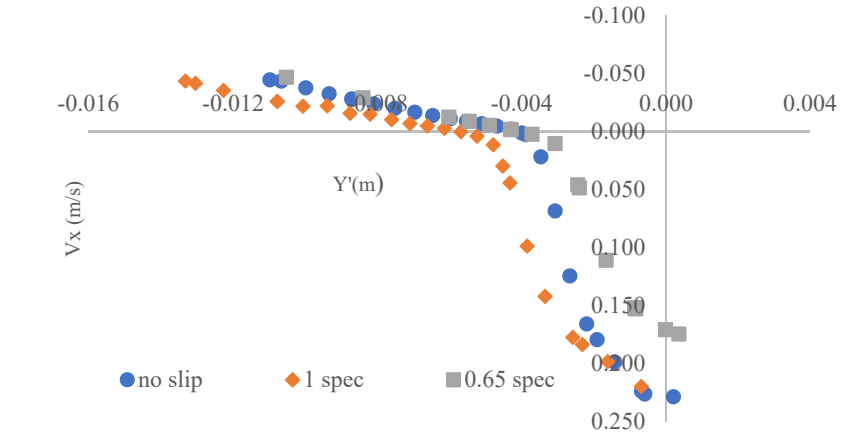

(**a**)

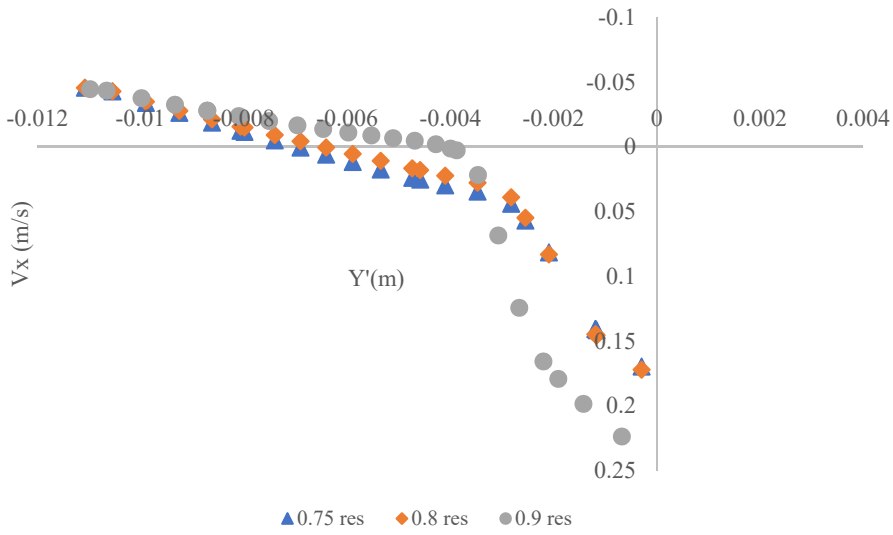

(**b**)

Figure 5. Streamwise velocity profiles for large particles with different: (**a**) boundary conditions (i.e., specularity coefficients 1 and 0.65 and no-slip); and (**b**) restitution coefficients (i.e., 0.9, 0.8, 0.75).

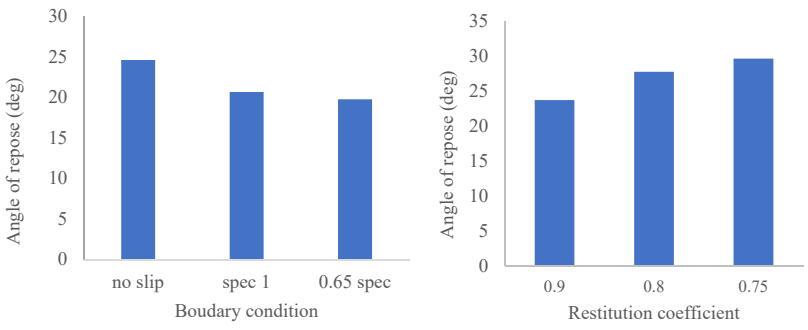

(**a**) (**b**)

Figure 6. Values of the repose angle at: (**a**) different specularity coefficients (1, 0.65) and no-slip boundary conditions; (**b**) different restitution coefficients (0.9, 0.8, 0.75).

3.2. Granular Pressure

Figure 7 shows the granular pressure distributions for large and small particles in the transverse plane at the middle location of the drum under three different combination of boundary condition and restitution coefficient. For small particles, the granular pressure is large in the middle region of the bed, where the particle segregation core forms. The fluctuation of granular pressure can be observed in the region due to particle collisions. The granular pressure has small values near the boundary of the rotating drum for small particles for the two cases with 0.9 restitution coefficient. For the case with the restitution coefficient of 0.75, a small region near the wall has the largest granular pressure. The pattern of the granular pressure distribution for larger particles is similar for all cases. The pressure has large values at a region near the wall where the large particle segregation band forms. It decreases with approaching the top of the flow and has small values in the middle region of the bed.

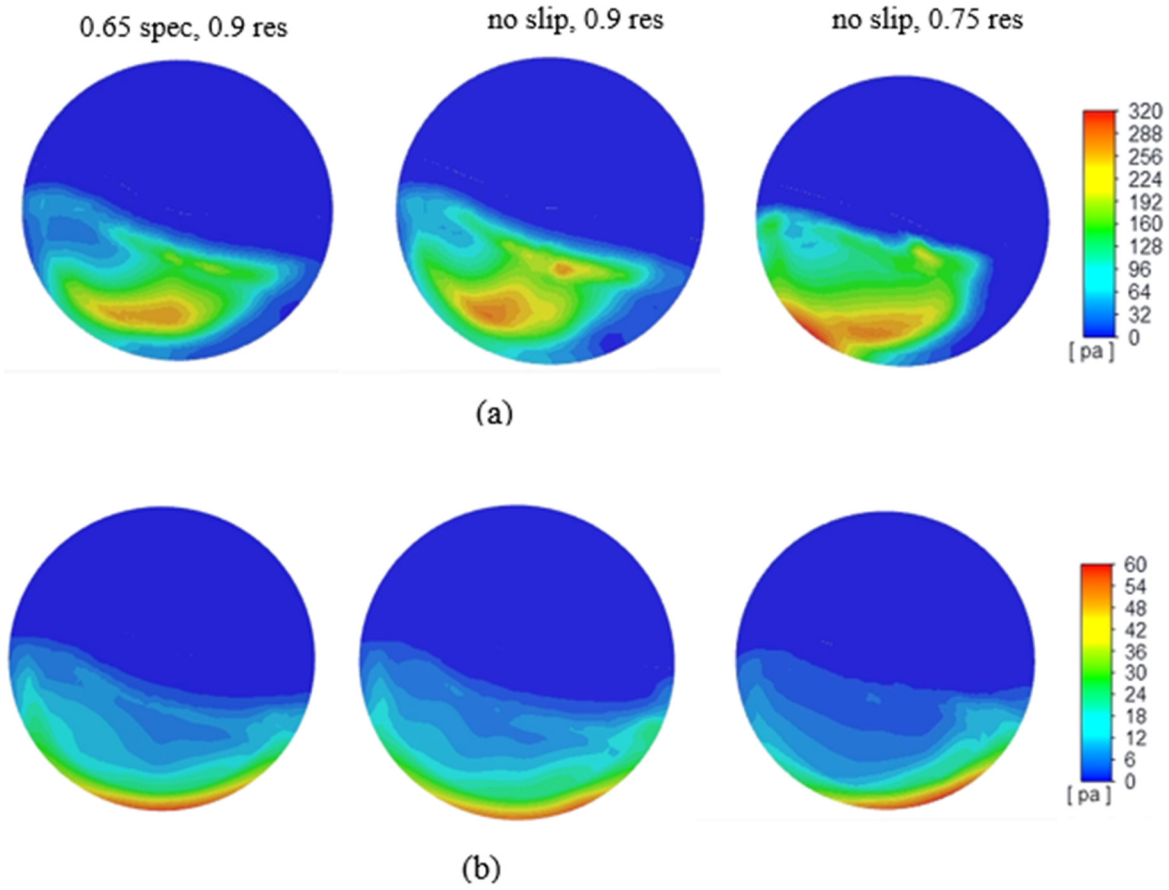

Figure 7. Distributions of granular pressure in the transverse plane at t = 5 s with different boundary conditions and restitution coefficients for: (**a**) small particles; and (**b**) large particles.

To quantify the effect of specularity coefficient on granular pressure, Figure 8 shows the variation of granular pressure with volume fraction at different boundary conditions. The whole drum has been considered. For small particles, as shown in Figure 8a, with increasing solid volume fraction, the granular pressure increases to reach a peak, decreases and then increases again. The reason for such a distribution pattern is because the granular pressure is highly related to particle collision. In the range of lower solid volume fraction, as the solid volume fraction increase, there is more chance for particles to collide with each other, thus resulting in a higher granular pressure. When such collision reaches its maximum, the granular pressure will decrease with the increase of solid volume fraction due to collision mechanism being impeded by more particles per unit volume. The quasi-

static contact plays a more important role at the stage. When the solid volume fraction increases further, the granular pressure increases due to the increase of the contact forces between particles. For large particles, as shown in Figure 8b, the granular pressure increases slowly and then sharply, with the increase of large particle volume fraction during the segregation process. The sharp increase in the granular pressure mainly occurs near the wall due to the formation of the segregation band. Furthermore, it can be seen that the granular pressure in the transverse plane for specularity 1 is higher than that for the no-slip boundary condition and 0.65 specularity coefficient for both large and small particles. This feature could be attributed to the large nonzero tangential velocity of the solid phase at the wall, i.e., strong interactions between the particles and wall for specularity 1 solid phase wall boundary condition compared with 0.65 specularity coefficient and the no-slip boundary condition. In addition, at a lower specularity coefficient and the no-slip boundary condition, some large particles remaining at the surface of the dense bed in the active region are hard to drop towards the bottom of the bed in the passive region. These large particles form a layer at the top of the bed and, thus, it takes more time to completely segregate for the no-slip boundary condition than specularity coefficient 1. For this reason, the granular pressure for specularity coefficient 1 is higher than the no-slip boundary condition at the same instant of time.

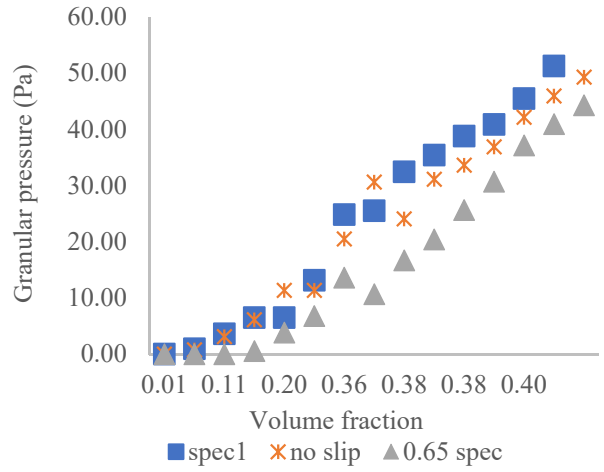

(**a**)

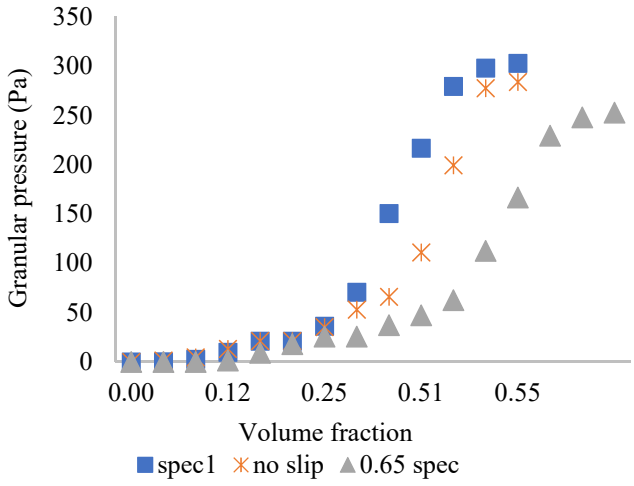

(**b**)

Figure 8. Variations of granular pressure with volume fraction under different boundary conditions for: (**a**) small particle, (**b**) large particle at t = 5 s.

Figure 9 shows the variations of granular pressure in the transverse plane at different distances to the end of the drum for small particle and large particles. Two distances, i.e., Z = 5 mm and 25 mm (middle location of the drum in the axial direction), have been considered. It can be seen that the case with specularity coefficient 1 has a higher granular pressure than that with the no-slip and 0.65 specularity coefficient boundary conditions, especially, for higher volume fraction. However, at the distance Z = 5 mm, the difference between the three boundary conditions is relatively small compared to the distance of Z = 25 mm, especially for large particles, which indicates that the boundary condition has a small effect near the ends of the drum, but relatively large effect far from the ends. In addition, the comparison of the granular pressures at different distances shows that for the same volume fraction, the granular pressure at Z = 25 mm is higher than that at the drum end for both small and large particles.

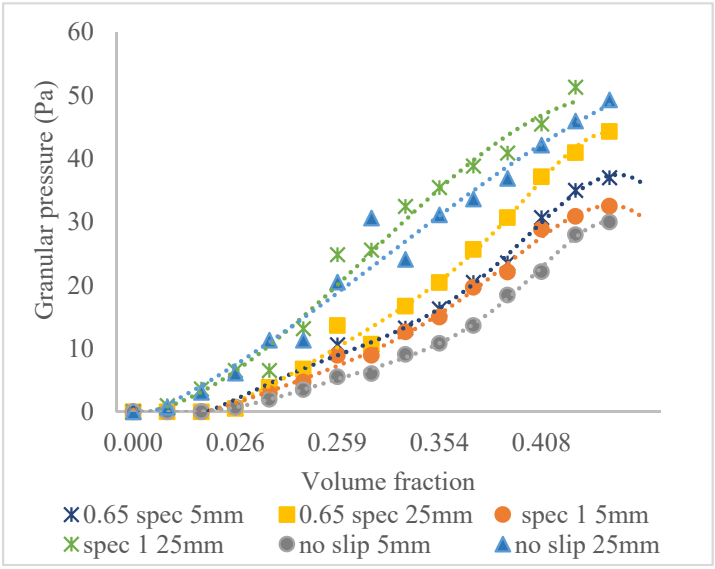

(**a**)

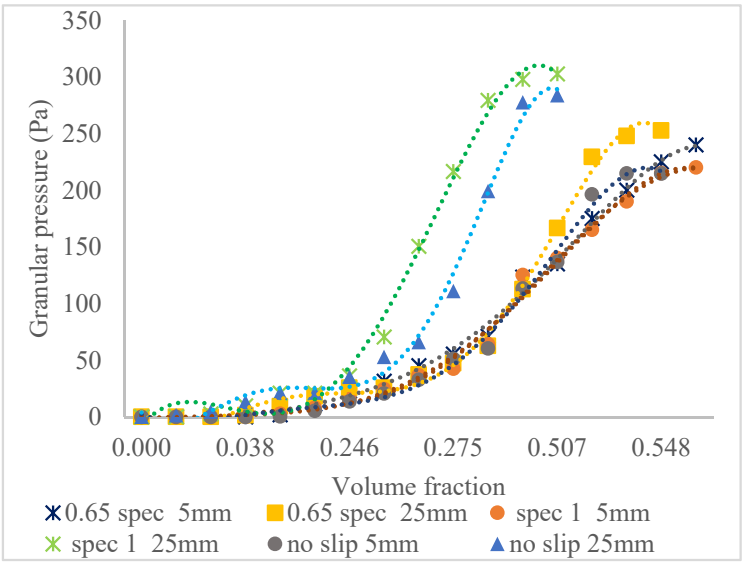

(**b**)

Figure 9. Variations of granular pressure on the transverse plane at two different locations Z = 5 mm and 25 mm for: (**a**) small particle, (**b**) large particle for different boundary conditions at t = 5 s.

Figure 10 shows the variation of granular pressure with volume fraction at different restitution coefficients with the no-slip boundary condition. Similar variation trend to Figure 8 can be observed for small and large particles for different restitution coefficients. The pressure exhibits an increase trend with the volume fraction for all cases. For small particles, there is a local peak. At the same volume fraction, the case with a higher restitution coefficient has a larger granular pressure. This is because a higher restitution coefficient would generate higher particle volume fractions along the radial direction and, thus, causes higher granular pressures.

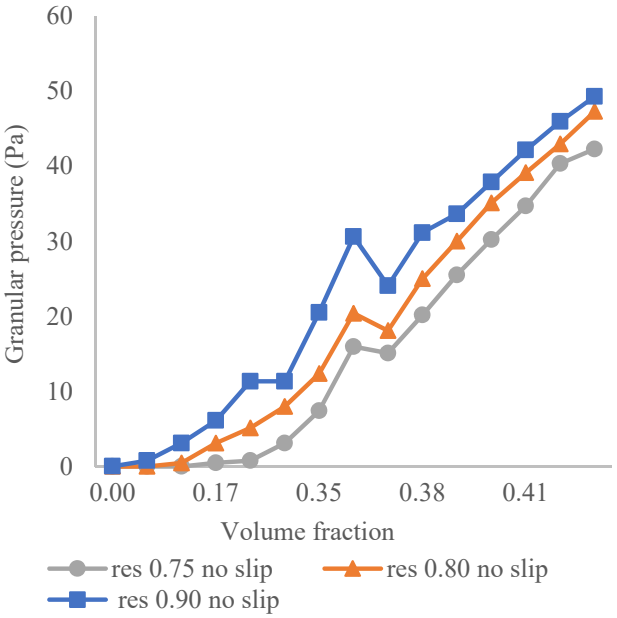

(**a**)

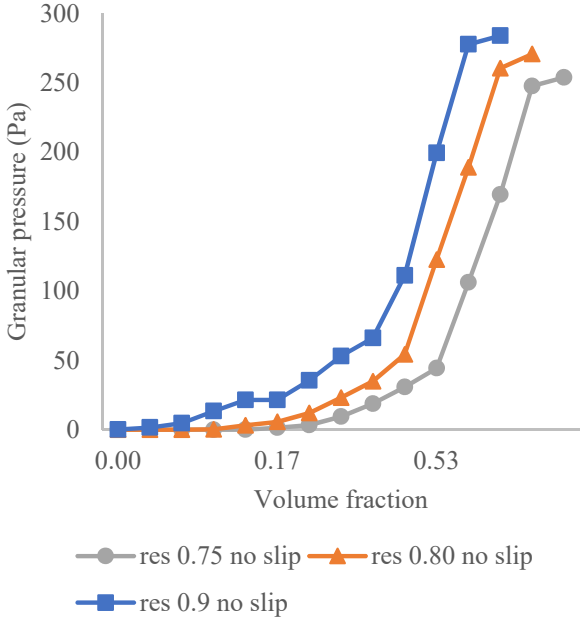

(**b**)

Figure 10. Variations of granular pressure with volume fraction for different restitution coefficients for: (**a**) small particle and (**b**) large particle at t = 5 s.

3.3. Granular Temperature

The granular temperature is an important concept in the hydrodynamics in gas—solid flows. It is related to the fluctuation of particle velocity. Figure 11 shows the granular temperature distributions in the YZ plane at X = 0 under different boundary conditions for small and large particles. There exists a temperature band near the bed surface in the active region where the particles exhibit a fluid like behaviour for all cases. In the region the band occupies, the volume fraction is low while the velocity is high, causing high collision between particles. As a result, high fluctuations of velocity occur, which lead to a high granular temperature. For large particles, the cases with specularity coefficient 1 and the no-slip boundary condition have a higher granular temperature than the case with specularity coefficient 0.65, which is due to the fact that the velocity at the active region is higher for the two conditions. In contrast, for small particles, specularity coefficient 0.65 has a higher granular temperature than other two conditions. At a lower specularity coefficient, the tangential forces between the particles and wall are high, which causes more collisions between particles and then increase the granular temperature in the active region.

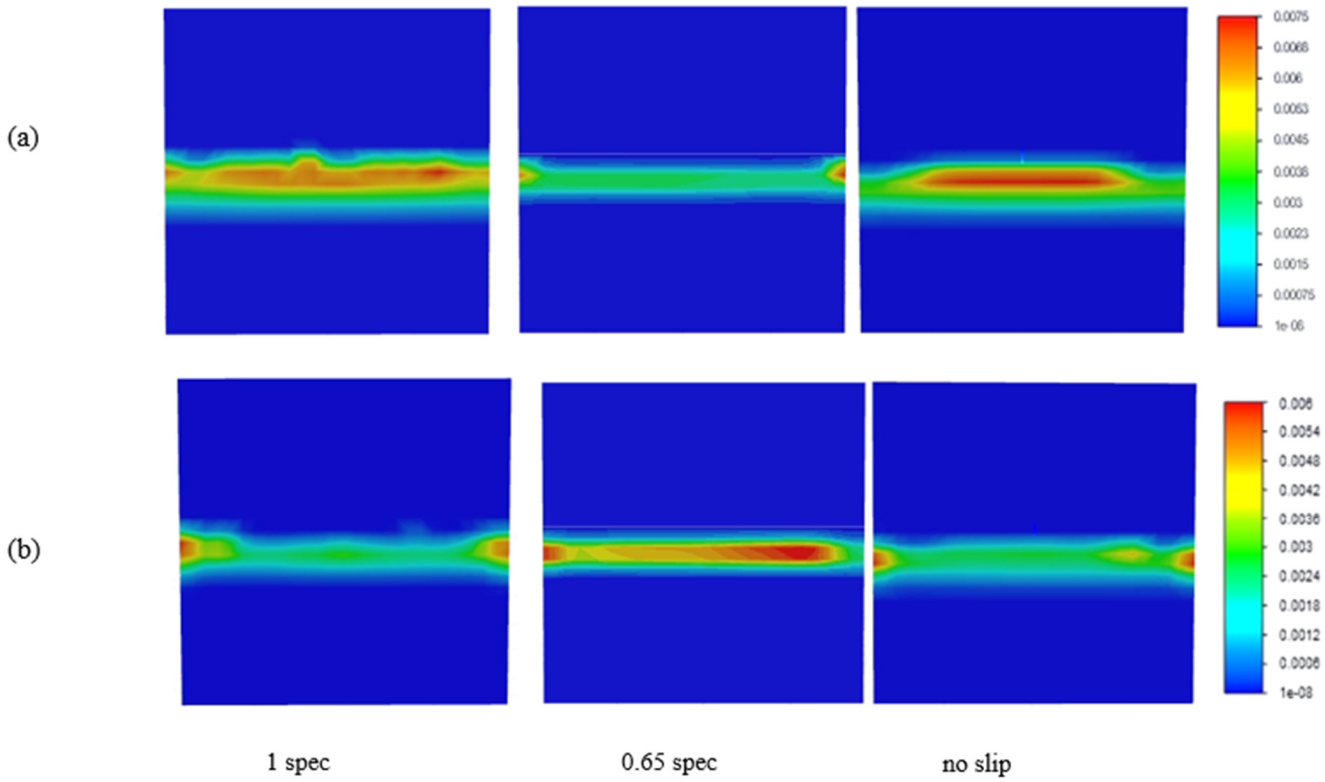

Figure 11. Distributions of granular temperature in the YZ plane at X = 0 under different boundary conditions at t = 5 s for: (**a**) large particles; and (**b**) small particles (The unit of granular temperature is m^2/s^2).

Figure 12 shows the variation of the granular temperature with volume fraction on the transverse plane at the middle location of the drum for different boundary conditions. The temperature increases with the volume fraction, reaches its peak and then decreases for both small and large particles. The peak with the high temperature corresponds to the temperature band near the bed surface as shown in Figure 11. For small particles, specularity coefficient 0.65 has the higher peak compared with the other two conditions, which is consistent with the finding in Figure 11b. The peak for specularity coefficient 1 is the lowest, which indicates that the area of the granular temperature band on the transverse plane is smaller than that of other two conditions. For large particles, the result is opposite. The specularity coefficient 1 condition generates the highest peak in the distribution of

temperature. The value of the volume fraction corresponding to the peak is relatively large for the condition as well. The small temperature at the small volume fraction can be attributed to the effect of the wall, near which both the volume fraction and the temperature are low.

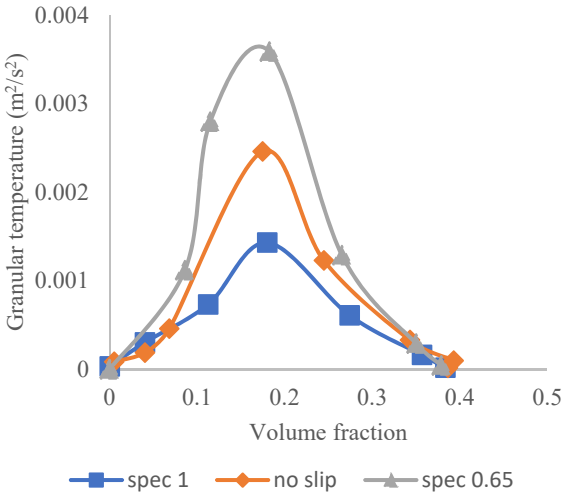

(**a**)

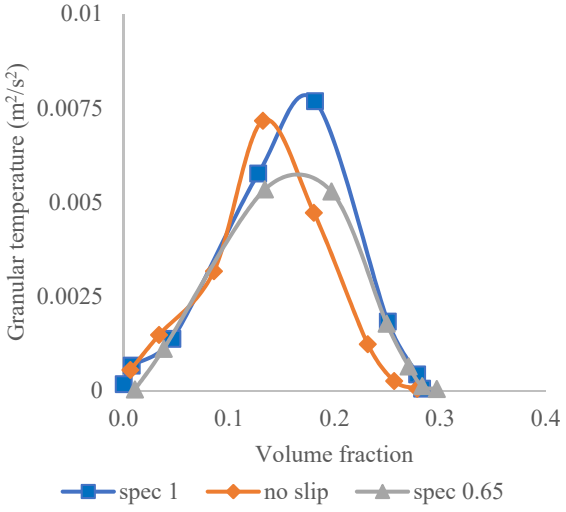

(**b**)

Figure 12. Variations of granular temperature with volume fraction at different boundary conditions for: (**a**) small particle; and (**b**) large particle at t = 5 s.

Figure 13 shows the variations of granular temperature alone the bed depth (i.e., along the Y′ axis, starting at the wall) for different values of restitution coefficient. For both small and large particles, the temperature is very small in the passive region, sharply increases along the depth to its peak in the active region and then decreases near the bed surface. The peaks correspond to the temperature bands. The reduction of temperature at the surface indicates that the particles move along the same direction at the surface, causing a small velocity fluctuation. Therefore, the temperature bands do not contain the bed surface and it should be beneath the surface. The no-slip boundary condition has been imposed on all cases. Due to the condition, there is a thin layer sticking to the drum wall, where the particles move with the rotation of the drum wall; therefore, there is a small temperature. The restitution coefficient affects the values of the temperature largely. Higher restitution coefficient would cause higher temperature at the same bed depth for both small and large particles. High restitution coefficient indicates a low dissipation rate of momentum at the

particles' collisions, resulting in the increment of particle fluctuation of the solid phase and, therefore, the increase in the value of granular temperature.

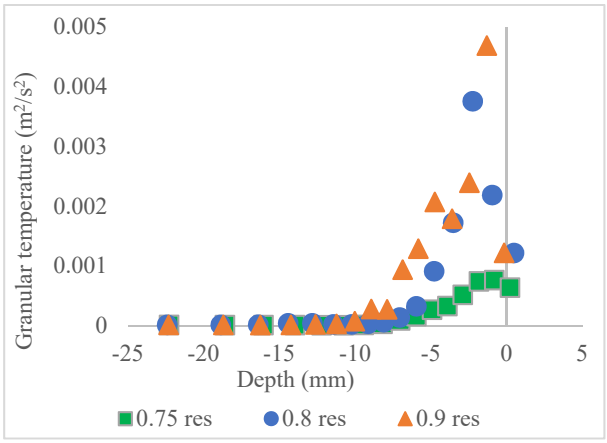

(**a**)

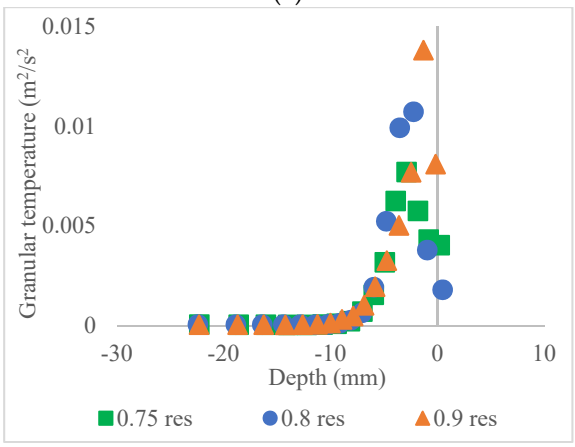

(**b**)

Figure 13. Granular temperature distributions along the bed depth for various restitution coefficients for: (**a**) small particles; and (**b**) large particles.

4. Conclusions

The dynamic segregation process of binary particles in a rotating drum has been simulated by using the CFD to examine the effect of the wall boundary condition and restitution coefficient on the hydrodynamic behaviour of the particles. The volume fraction, velocity, angle of repose, granular pressure, granular temperature for small and large particles have been considered. The main conclusions can be summarized as follows.

- The segregation pattern is similar to that obtained in the previous studies: small particle forming a segregation core at the centre and large particles forming a segregation band near the wall. Correspondingly, high granular pressure exists at the centre region for small particles and near the wall for large particles. There is a granular temperature band below the bed surface in the active region of the flow.
- The comparison of the no-slip boundary condition and specularity coefficient 1 shows that the values of the properties considered are different under the two conditions. In particular, the case with no-slip boundary condition has a lower depth of active region, a higher angle of repose than that for the boundary condition with specularity coefficient 1. Further, the no-slip condition would cause lower granular pressure for both small and large particles and higher granular temperature for small particles. These results indicate that the specularity coefficient of 1 cannot be considered to be the no-slip boundary condition in the simulations of gas–solids flow.

- The boundary condition affects the magnitudes of the properties considered, although its influence on the distribution pattern of these properties is limited. Increasing the specularity coefficient would lead to an increase in the active region depth, angle repose, granular pressure for both small and large particles and granular temperature for large particles, but a decrease in granular temperature for small particles at the same volume fraction.
- The restitution coefficient between particles plays an important role in granular pressure, granular temperature and angle of repose and, consequently, affect the formation of segregation in the rotating drum. With increasing restitution coefficient, the angle of repose decreases and granular pressure and temperature increase at the same volume fraction for both small and large particles.

The results indicate that proper specularity coefficient and restitution coefficient should be selected to achieve an effective segregation process. Future work will be conducted to develop approaches to determine the values of these properties, especially specularity coefficient for specific systems, which is hard to be obtained by physical experiments.

Author Contributions: Conceptualization, R.R., H.Z. and A.Y.; methodology, R.R. and H.Z.; software, R.R.; validation, R.R.; formal analysis, H.Z. and R.R.; investigation, R.R.; resources, H.Z.; data curation, R.R.; writing—original draft preparation, R.R.; writing—review and editing, H.Z.; visualization, R.R.; supervision, H.Z. and A.Y.; funding acquisition, H.Z. and A.Y. All authors have read and agreed to the published version of the manuscript.

Funding: This research was funded by ARC Research Hub for Computational Particle Technology (the Australian Research Council, Jiangsu Industrial Technology Research Institute and Western Sydney University), grant number ARC IH140100035.

Institutional Review Board Statement: Not applicable.

Informed Consent Statement: Not applicable.

Conflicts of Interest: The authors declare no conflict of interest.

References

1. Huang, A.N.; Kuo, H.P. Developments in the tools for the investigation of mixing in particulate systems—A review. *Adv. Powder Technol.* **2014**, *25*, 163–173. [CrossRef]
2. Santos, D.A.; Petri, I.J.; Duarte, C.R.; Barrozo, M.A.S. Experimental and CFD study of the hydrodynamic behavior in a rotating drum. *Powder Technol.* **2013**, *250*, 52–62. [CrossRef]
3. Widhate, P.; Zhu, H.P.; Zeng, Q.H.; Dong, K. Mixing of particles in a rotating drum with inclined axis of rotation. *Processes* **2020**, *8*, 1688. [CrossRef]
4. Mellmann, J. The transverse motion of solids in rotating cylinders—Forms of motion and transition behavior. *Powder Technol.* **2001**, *118*, 251–270. [CrossRef]
5. Kuo, H.P.; Tseng, W.T.; Huang, A.N. Controlling of segregation in rotating drums by independent end wall rotations. *KONA Powder Part. J.* **2016**, *33*, 239–248. [CrossRef]
6. Hogg, R. Mixing and segregation in powders: Evaluation, mechanisms and processes. *KONA Powder Part. J.* **2009**, *27*, 3–17. [CrossRef]
7. Karunarathne, S.S.; Jayarathna, C.K.; Tokheim, L. Mixing and segregation in a rotating cylinder: CFD simulation and experimental study. *Int. J. Model. Optim.* **2017**, *7*, 1–6.
8. Kotoky, S.; Dalal, A.; Natarajan, G. Effects of specularity and particle-particle restitution coefficients on the hydrodynamic behavior of dispersed gas particle flows through horizontal channels. *Adv. Powder Technol.* **2018**, *29*, 874–889. [CrossRef]
9. Santos, D.A.; Duarte, C.R.; Barrozo, M.A.S. Segregation phenomenon in a rotary drum: Experimental study and CFD simulation. *Powder Technol.* **2016**, *294*, 1–10. [CrossRef]
10. Johnson, P.C.; Jackson, R. Frictional-collisional constitutive relations for granular materials, with application to plane shearing. *Fluid Mech.* **1987**, *176*, 67–93. [CrossRef]
11. Huang, A.N.; Kuo, H.P. CFD simulation of particle segregation in a rotating drum. Part I: Eulerian solid phase kinetic viscosity. *Adv. Powder Technol.* **2017**, *28*, 2094–2101. [CrossRef]
12. Hussainova, I.; Kübarsepp, J.; Shcheglov, I. Investigation of impact of solid particles against hard metal and cermet targets. *Tribol. Int.* **1999**, *32*, 337–344. [CrossRef]
13. Labous, L.; Rosato, A.D.; Dave, R.N. Measurements of collisional properties of spheres using high speed video analysis. *Phys. Rev. E* **1997**, *56*, 5717–5725. [CrossRef]

14. Lu, H.; Gidaspow, D. Hydrodynamics of binary fluidization in a riser: CFD simulation using two granular temperatures. *Chem. Eng. Sci.* **2003**, *58*, 3777–3792.
15. Santos, D.A.; Dadalto, F.O.; Scatena, R.; Duarte, C.R.; Barrozo, M.A.S. A hydrodynamic analysis of a rotating drum operating in the rolling regime. *Chem. Eng. Res. Des.* **2015**, *94*, 204–212. [CrossRef]
16. Delele, M.A.; Weigler, F.; Franke, G.; Mellmann, J. Studying the solids and fluid flow behavior in rotary drums based on a multiphase CFD model. *Powder Technol.* **2016**, *292*, 260–271. [CrossRef]
17. Huang, A.N.; Kuo, H.P. CFD simulation of particle segregation in a rotating drum. Part II: Effects of specularity coefficient. *Adv. Powder Technol.* **2018**, *28*, 3368–3374. [CrossRef]
18. Machado, M.V.C.; Nascimento, S.M.; Duarte, C.R.; Barrozo, M.A.S. Boundary conditions effects on the particle dynamic flow in a rotary drum with a single flight. *Powder Technol.* **2017**, *311*, 341–349. [CrossRef]
19. Taghizadeh, A.; Hashemabadi, S.H.; Yazdani, E.; Akbari, S. Numerical analysis of restitution coefficient, rotational speed and particle size effects on the hydrodynamics of particles in a rotating drum. *Granular Matter* **2018**, *20*, 56. [CrossRef]